Journal of Imaging Science and Technology® 53(5): 050201–050201-6, 2009.

Absorption Mechanism of Aqueous and Solvent Inks into Synthetic Nonwoven Fabrics

Hitomi Hamada
Research Institute, National Printing Bureau of Japan, Odawara, Kanagawa 256-0816, Japan
E-mail: hamada@res.npb.go.jp

Douglas W. Bousfield and Wing T. Luu
Department of Chemical and Biological Engineering, University of Maine, Orono, Maine 04469-5737

Abstract. *In order to obtain high quality printing results, it is important to understand the mechanisms of ink absorption and setting on various substrates. The final position of ink pigments determines the ink density and the resolution of the printed product. Absorption rates of aqueous and solvent inks into nonwoven fabrics were characterized with a Bristow absorption wheel. A model based on Darcy's Law was applied to predict the ink absorption rate into the nonwoven fabrics. The model links the void fraction, pore size, contact angle, and the Darcy permeability coefficients to the absorption rate. The results showed a good correlation between the experimental data and the predicted results for many combinations of substrates and inks, but in a few cases, the absorption rates were different than expected. A clear difference of microscale distributions between aqueous and solvent inks on the nonwoven fabrics could be obtained by confocal laser scanning microscopy. © 2009 Society for Imaging Science and Technology.*
[DOI: 10.2352/J.ImagingSci.Technol.2009.53.5.050201]

INTRODUCTION

The mechanisms of ink absorption and setting on porous materials such as paper, for all kinds of printing methods, determine the rate of printing and influence the final quality of the print. Recently, not only coated and uncoated papers but also nonwoven fabrics, synthetic fiber paper, and films have been used as materials for printing. The surface characteristics of these substrates influence the ink setting rate and quality of printing, but the relationship between the final pigment deposition and the rate of absorption has not been quantified.

The liquid flow in a porous substrate has been shown, in many cases, to follow Darcy's Law which states that the rate of flow is proportional to the pressure gradient and inversely proportional to viscosity. Much work has been done in the area of modeling fluid motion in porous media. If the pressure driving force is given by the Laplace equation and the resistance to flow is described by the flow in a capillary, the Lucas–Washburn equation is found to describe the behavior; this equation is based on a series of parallel capillaries all of the same radius.[1] Often, various correction terms are used to fit the results to experimental data. A three-dimensional (3D) model that describes the flow in layered porous media has been described.[2] The model could predict some sets of experimental data for a coating layer on a paper, measuring the properties of each separately. A model by Bousfield and Karles[3] based on the pore connectivity and pore size was proposed that seems to give good comparison with experiments.

The main purpose of early research using a confocal laser scanning microscope (CLSM) in the printing industry was to characterize surface roughness.[4] The surface profiles of matte-coated paper were measured three dimensionally using CLSM and were related to the perception of gloss.[5] CLSM has been shown to be a powerful tool to characterize ink penetration into coated and uncoated papers utilizing a fluorescence stain technique.[6,7] It was reported to be possible to characterize ink pigment position within printed newsprint sheets by the image analysis techniques of CLSM.[8] The penetration of dye-based inks for ink jet has been studied by CLSM.[9] The process of pigment type ink setting on noncellulose fibers was investigated using CLSM: it was confirmed that the ink setting differed by the particle size of the pigment.[10] Furthermore, they succeeded in detecting the fluorescence of the cyan ink, which did not emit fluorescence by a visible laser, using an ultraviolet laser equipped with the CLSM. The microscale distribution of dye and pigment type inks on corona-treated nonwoven fabrics was evaluated by CLSM. Microstructural changes of the sheet surface had a great influence on the ink setting and distribution.[11]

In this paper, the rates of ink absorption into nonwoven fabrics were characterized with a common absorption test method. The absorption rate was predicted using Darcy's Law with the pressure gradient given by the Laplace equation. The microscale distribution of inks on nonwoven fabrics was investigated by CLSM. Clear differences in rates and pigment deposition were seen for the different substrates between aqueous and solvent inks.

MATERIAL AND METHODS

Samples

Three kinds of synthetic nonwoven fabrics were used. The sheet named PVA (12 g/m^2) was made from polyvinyl alcohol (PVA) fibers by a wet process. Another sheet named PP-A (15 g/m^2) was made from polypropylene (PP)

Received Dec. 12, 2008; accepted for publication Jun. 24, 2009; published online Aug. 11, 2009.
1062-3701/2009/53(5)/050201/6/$20.00.

fibersand polyvinyl alcohol fibers mixed. The sheet named PP-AC (18 g/m^2) comprised the PP-A sheet coated with acrylic latex (Nippon Zeon, Japan).

Aqueous and solvent inks for flexographic printing (T&K, TOKA, Japan) were compared. The aqueous ink is composed of 20% red pigment, 9% isopropyl alcohol, 15% acrylic resin, 55% water, and 1% other additives. The solvent ink is composed of 15% red pigment, 20% of a mixture of resin, 62% of a mixture of alcohols as solvent, and 3% other additives. The same type of azo pigment is used in both inks. The viscosity of aqueous and solvent inks was 0.50 and 0.15 Pa s, respectively, at the shear rate of 10 s^{-1} and 25°C, as measured by a rheometer (CVO, Bohlin Instruments).

Characteristics of Nonwoven Sheets

The pore volume of nonwoven sheets was determined by the silicone oil void test. Silicone oil was applied to the samples to ensure that they were saturated with oil. The oil was wiped from the surface. The void fraction was calculated from the area and weight of the samples before applying the oil and the weight of oil saturated samples. The void fraction was also estimated using CLSM: the oil-filled volume in the sheets was measured by image analysis. The silicone oil was stained with a fluorescent agent, Nile Red, before measurement.

The contact angle of a water or oil drop on the nonwoven sheets was also measured. After dropping liquid on the nonwoven sheet, a camera recorded the contact angle change in the liquid drop on the substrate every 10 ms for 300 ms. The roughness of the sheet surfaces was evaluated by measuring the surface profile of each sheet using CLSM.

A mercury porosimeter (Auto Pore IV 9500, Micromeritics Instrument Co.) was used to determine the pore sizes in the nonwoven sheets. Pore size distributions were also estimated from CLSM images by measuring the oil-filled area in the oil saturated sheets and image analysis.

Ink Absorption Rate into Nonwoven Sheets

The absorption rates of aqueous and solvent inks into nonwoven sheets were characterized with a Bristow absorption wheel. A known volume of ink diluted to 10 wt % was added to the trough. (The inks had to be diluted to enable them to flow easily through the slit at the bottom of the trough.) The viscosity of diluted inks was nearly equal to that of water. The area of the trace left on the substrate was measured. The contact time between the ink and the substrate was varied by changing the speed of the wheel. In some cases, several layers of the paper were needed to prevent the "saturation" of the sample. The volume absorbed per unit area was then calculated.

A model based on the Laplace equation and Darcy's law was used to predict ink absorption rate into the nonwoven sheets. Darcy's law assumes that the rate of flow (v) in any porous material is given by

$$v = \frac{K\Delta P}{\mu L}, \tag{1}$$

where K is the permeability coefficient that depends on the structure of the porous material, ΔP is the pressure difference over length (L), and μ is the fluid viscosity. The velocity is equal to the volumetric flow rate per unit area, $v = d(V/A)/dt$. For the case of a fluid penetrating into a planar material in the thickness direction, the depth of penetration can be linked to the volume of penetration by a mass balance of

$$LA\varepsilon = V, \tag{2}$$

where ε is the void fraction of the material. This expression can be used to eliminate the penetration depth (L) from Eq. (1).

If fluid is absorbing into a porous material, the Laplace equation should predict the pressure driving force given as

$$\Delta P = \frac{2\sigma \cos(\theta)}{R}, \tag{3}$$

where σ is the surface tension, R is the pore radius in the material, and θ is the contact angle. Eliminating pressure from Eq. (1) and integrating the result with respect to time gives

$$\frac{V}{A} = \sqrt{\frac{4K\varepsilon \cos(\theta)\sigma t}{\mu R}}, \tag{4}$$

where V/A is the ink absorption volume per unit area. This expression is similar to the Lucas–Washburn equation except that the resistance to flow is expressed in a general way, not as a function of pore size. The contact angle, void fraction, and pore radius were obtained from experiments, while the surface tension and viscosity were assumed to be the same as water for the aqueous inks.

Real samples have a distribution of pore sizes. There is no clear radius to use in Eq. (4). A simple way to include a distribution of radii is to use the porosity results in different radius size classes. For each size class, the volume of pores is known from the porosity data. Therefore, a void fraction (ε_i) can be calculated for each radius size class (R_i). The absorption amount is assumed to be a summation of the absorption of each size class as

$$\frac{V}{A} = \sqrt{\sum \frac{4K\varepsilon_i \cos(\theta)\sigma t}{\mu R_i}}. \tag{5}$$

The permeability coefficient (K) was obtained by measuring the water and air permeability through the sample based on this form of Darcy's Law,

$$\frac{d(V/A)}{dt} = \frac{K\Delta P}{\mu T}, \tag{6}$$

Table I. Measured parameters of substrates.

		PVA	PP-A	PP-AC
Thickness (μm)		45	58	68
Void fraction	ε	0.44	0.38	0.36
Contact angle, water	θ_w	74	90	74
Contact angle. oil	θ_o	9.3	7.3	7.5
Permeability, water ($m^2 \times 10^{-12}$)	K_w	0.9	1.1	0.8
Permeability, air ($m^2 \times 10^{-12}$)	K_a	2.7	3.4	3.8
Permeability, air, wet. condition ($m^2 \times 10^{-12}$)	K_{aw}	0.08	0.12	0.11

where ΔP is the pressure drop across the entire sample and T is the thickness of the sample that the pressure acts in the flow direction. Water permeability (K_w) and air permeability (K_a) were obtained by measuring the volume of water or air volume passing through a given area of nonwoven sheet in unit time. The air permeability for samples wetted by water (K_{aw}) was also measured. The samples were immersed in water for 1 min and then the volume of air passing through the wetted samples was measured.

Observation by CLSM

A CLSM (TCS-SP2, Leica) was used in this experiment. The sample saturated with oil dyed with Nile Red was first scanned with a laser beam, and the fluorescence emitted from the dye in the sample was detected as a fluorescence image. An excitation wavelength of 514 nm from an Ar laser (50 mW) was used for this analysis. A 3D image was reconstructed from a series of single confocal images accumulated digitally.

The selected objective lenses were a 20× dry lens for measuring surface profiles and a 40× oil-immersion lens with immersion oil (refractive index 1.518) for observing ink distributions. The Z-resolution of the oil-immersion lens is three times better than that of a dry lens with air between the sample and the objective lens. Therefore, it is possible to reduce the optical resolution for a depth to less than 0.6 μm using the oil-immersion lens.[12] Oil-immersion lenses have been previously used to observe pulp fibers.[13,14] Confocal images were obtained using XYZ scan modes. A sequence of XY frames (238×238 μm^2) was obtained at 0.5 μm intervals in the thickness direction. The pixel count of each frame was 1024×1024 pixels.

RESULTS AND DISCUSSION

Characteristics of Nonwoven Sheets

Table I shows the properties of the nonwoven sheets. In the silicone oil test results, the PVA sheet showed the highest void fraction (ε), while the PP-AC sheet had the lowest value because it was coated with latex. The void fraction obtained by CLSM measurements showed a value close to the results obtained by the silicone oil test.

Table II. Surface profile of substrates by CLSM.

		PVA	PP-A	PP-AC
Maximum amplitude	μm	43	27	35
Minimum amplitude	μm	3.3	7.6	6.5
Standard deviation		13	5.8	9.0
Variance		177	34	92

The contact angle (θ) measured at 10 ms is shown in Table I. The PVA sheet showed the lowest water contact angle because the PVA fiber is hydrophilic. The PP-A sheet showed the highest water contact angle because polypropylene fiber contained in the PP-A sheet is hydrophobic. Comparing the PP-A sheet with the PP-AC sheet, we observed that the water contact angle decreased after coating with acrylic latex whereby the surface became more hydrophilic. The oil contact angle test showed very low values; the PVA sheet showed a slightly higher value than the PP-A and PP-AC sheets.

The hydrophilic PVA sheet showed lower permeability despite of its high void fraction, and the hydrophobic PP-A sheet exhibited higher permeability. This result is hard to understand but must be related to the connectivity of the pores. The water permeability was lower than the air permeability for the dried samples. This difference may come from a small structural change that occurs when the samples are in contact with water; alternatively the air permeability measurement may have a large margin of error because of very fast air flow. The air permeability for the wetted samples was lower than the water permeability. This result may mean that water contacting substrates affects the permeability; however, fiber swelling by water was not observed.

Table II shows the surface profiles of the nonwoven sheets measured by CLSM. The standard deviation and variance calculated from the amplitudes are correlated with the roughness of the sheets. The PVA sheet showed the highest standard deviation and variance, which means that the surface of PVA sheet is the roughest.

Figure 1 shows pore size distributions in the sheets measured by the mercury porosimeter. It is clear that all samples have a wide range of pore sizes. The uncoated PVA and PP-A sheets have larger pores up to 20 μm of diameter. In the coated PP-AC sheet, there were many smaller pores between 0.1 and 5 μm. This is because larger pores were filled up with the latex. Figure 2 shows the cumulative pore volume. The PP-A sheet showed the highest pore volume, which did not agree with the silicone oil test results. However, the data in the region larger than 100 μm might not be reliable because of the method to hold the sample in the porosimeter, and the region larger than thickness of samples does not seem to show the pores in the sheets. Therefore, the region larger than the thickness of the sheets was ignored for the prediction of absorption rate. The results from image analysis using the CLSM images corresponded with these results.

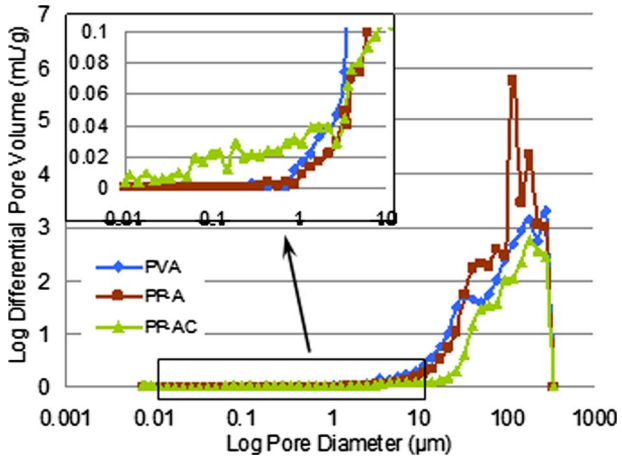

Figure 1. Pore size distributions in the nonwoven sheets.

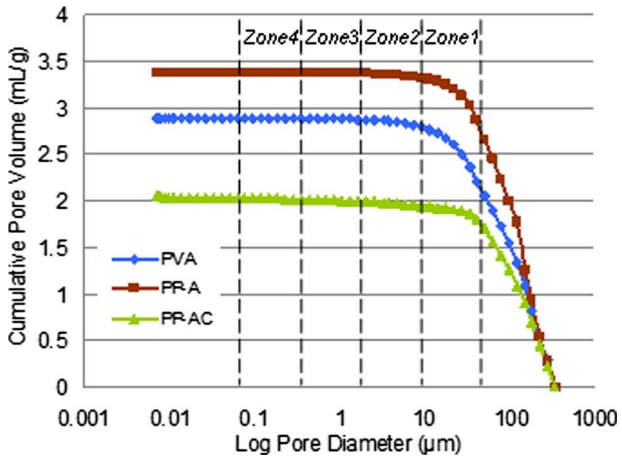

Figure 2. Cumulative pore volume in the nonwoven sheets.

Ink Absorption Rate into Nonwoven Sheets

Figures 3–6 show total liquid volume (TLV) transferred to the sheets per unit area by measuring with the Bristow absorption wheel and predictions using Darcy's Law; this volume is also related to the penetration depth of fluid into the sample. Figs. 3 and 4 show the aqueous ink results, and Figs. 5 and 6 present the solvent ink results. Solid lines represent experimental data and dotted lines are the predicted results.

The solvent ink penetrated deeper into the sheets than the aqueous ink at the same contact time for all samples. Ink penetration depth into the PP-A sheet was the lowest for the aqueous ink but was the highest for the solvent ink. The aqueous ink apparently spread over the surface of the PVA sheet and did not penetrate deeply into the sheet because the surface is hydrophilic and permeability is low. These results demonstrate that a combination of contact angle and permeability control penetration.

Comparing the PP-A sheet with the PP-AC sheet, we find that the penetration depth of aqueous ink increases with acrylic latex coating. It was observed by CLSM that the coated latex penetrated to the bottom of the sheets. The aqueous ink may therefore penetrate deeply into the PP-AC sheet in regions where the latex has also penetrated.

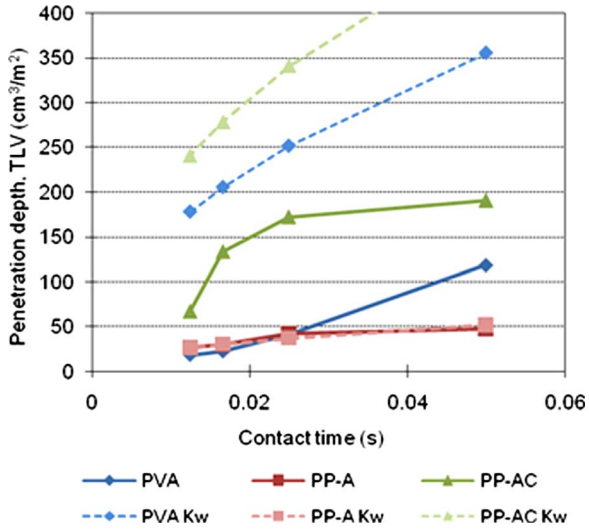

Figure 3. The absorption rates of aqueous ink. Solid lines: experimental. Dotted lines predicted by K_w.

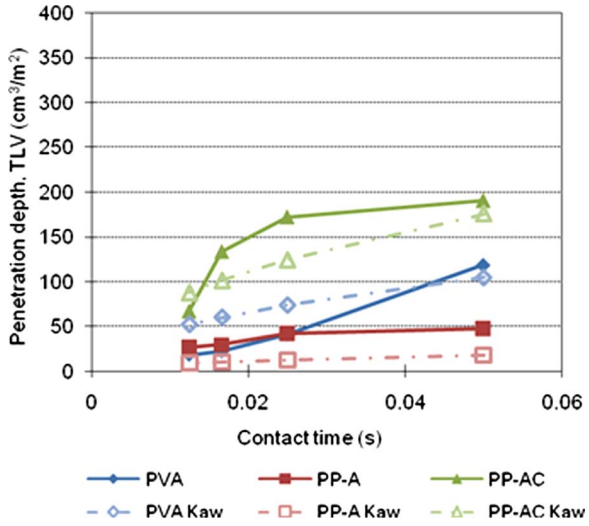

Figure 4. The absorption rates of aqueous ink. Solid lines: experimental. Dotted lines predicted by K_{aw}.

Modeling Ink Absorption Rate

The predicted absorption rates for the aqueous ink were derived from Eq. (5). The experimental data for the water permeability coefficient (K_w), the air permeability coefficient under wet condition (K_{aw}), the water contact angle (θ_w) shown in Table I, and the literature data for water surface tension (σ), 0.07 N/m, and viscosity (μ), 0.001 Pa s, were used for the prediction. The void fraction (ε_i) was calculated for each radius size class (R_i) in four radius size classes: zones 1–4 as shown in Fig. 2. The regions lager than each sheet thickness and smaller than 0.1 μm were ignored. The resulting void fraction data are shown in Table III.

The predicted absorption rates for the aqueous ink, derived using the water permeability (K_w) are shown in Fig. 3. The results showed a high correlation between the experimental data and the results predicted for the PP-A sheet. This demonstrates that the model captures the correct relationship among contact angle, pore size, and permeability.

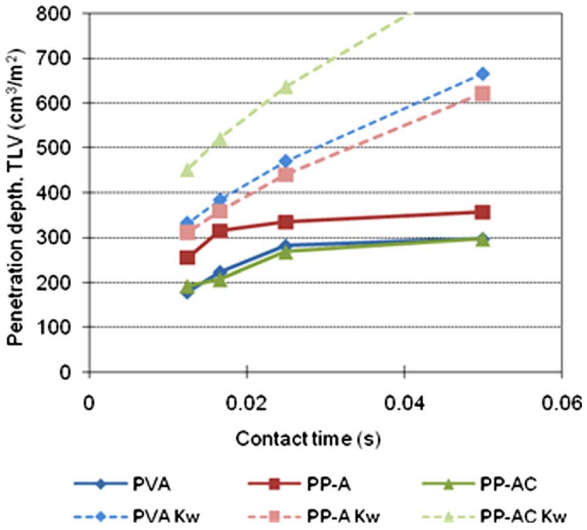

Figure 5. The absorption rates of solvent ink. Solid lines: experimental. Dotted lines predicted by K_w.

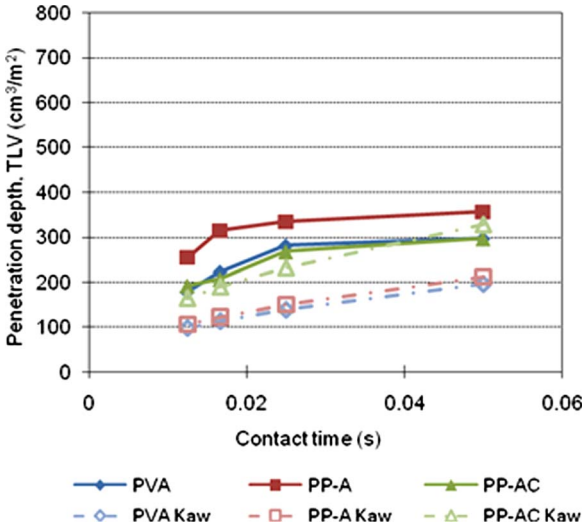

Figure 6. The absorption rates of solvent ink. Solid lines: experimental. Dotted lines predicted by K_{aw}.

However, for the cases of the PVA and PP-AC sheets, the predictions were higher than experimental. This difference may be caused by ink trapped in the space between the piled sheets, which led to decrease in the absorption depth. According to the surface profiles by CLSM shown in Table II, the surfaces of PVA and PP-AC sheets were rougher than PP-A sheet. For the predicted results, the low values of absorption rate in PP-A were attributed to the high contact angle. The high values for the PVA and PP-AC sheets were attributed to the combination of low contact angle and medium permeability coefficient.

If the values of the air permeability under wet condition (K_{aw}) were used for prediction, the predicted results became closer to the experimental data for the PVA and PP-AC sheets as shown in Fig. 4. These results show that the prediction is strongly influenced by the permeability coefficient. During the measurements of water permeability, water may leak due to the structure of the equipment. If the water permeability decreases, the predicted results are likely to be closer to the experimental data. This approach could be applied to predict liquid absorption rate into porous media such as synthetic nonwoven sheets.

The predictions for the solvent ink shown in Figs. 5 and 6 were obtained from water permeability (K_w) and air permeability under wet condition (K_{aw}), respectively. Oil contact angle (θ_o) was also used for the prediction of solvent ink absorption. When water permeability was used, the predicted results were higher than experimental. The predicted results were closer to the experimental data when air permeability under wet conditions was used. If more accurate permeability and/or contact angle are available, the predicted results may become closer to the experimental data.

The predicted results calculated from the peak value of pore radius and the average void fraction, instead of the summed void fraction in different radius size classes, do not correlate with the experimental data. Air permeability (K_a) also was used to predict absorption rate; however, the calculated data did not match the experimental data.

Ink Distribution on Nonwoven Sheets Observed by CLSM

Figures 7–9 are the reconstructed images for the nonwoven sheets with (1) aqueous and (2) solvent inks applied by Bristow absorption wheel. The center image is one of the *XY*-plane stacked images. The bottom image is an *XZ*-plane which is sectioned virtually along line 1, and the right image is a *YZ*-plane which is sectioned along line 2. The red ink emitted strong fluorescence at the excitation wavelength of 514 nm and is shown as bright color. The fibers did not emit any fluorescence at this wavelength.

For the hydrophilic PVA sheet, the aqueous ink spread over the surfaces of each fiber and evenly covered the PVA fibers of a concave shape as shown in Fig. 7. In contrast, for the solvent ink, the pigment particles in the ink were aggregated and were unevenly distributed on the PVA fibers. It seems that the pigment particles are not dispersed well in the solvent and the solvent evaporates rapidly. As a result the aggregate pigments are fixed on the fibers.

Figure 8 shows the results with the PP-A sheet. Similar to previous results with the PVA sheet, the aqueous ink spread over and covered the surfaces of each fiber. The pigment particles in the solvent ink were more aggregated than on the PVA sheet.

The pigment particles in solvent ink were also aggregated on the PP-AC sheet as shown in Fig. 9. Most of the aqueous ink tends to be distributed on the coated latex. This result supports the hypothesis that the aqueous ink penetrates into regions where there is hydrophilic latex in the PP-AC sheet. The cross-section images show that the pigments in ink are captured by latex coating near the surface and also show that the solvent ink pigments seem to be deposited in a distinct layer. The latex may be able to "filter" the ink pigments because of the small pore size, as shown in Fig. 1. It is not clear why the solvent inks seem to produce a distinct ink layer while the aqueous inks do not on the PVA and PP-A sheets.

Table III. Void fraction in different radius size classes.

			Zone 1	Zone 2	Zone 3	Zone 4
Pore radius	R_i (μm)	PVA	11.9	2.54	0.54	0.094
		PP-A	13.7	2.54	0.54	0.094
		PP-AC	15.7	2.54	0.54	0.094
Void fraction	ε_i	PVA	0.19	0.028	0.003	7.9×10^{-5}
		PP-A	0.22	0.015	0.002	3.1×10^{-5}
		PP-AC	0.14	0.013	0.007	0.0042

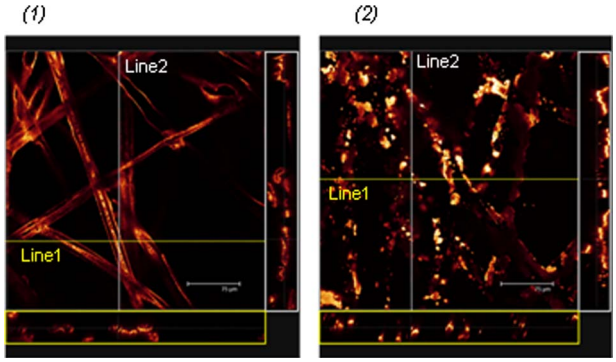

Figure 7. The reconstructed images of the orthogonal projections for the PVA sheet printed with the (1) aqueous and (2) solvent inks.

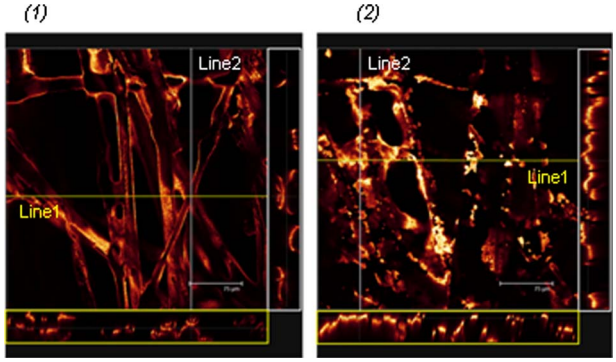

Figure 8. The reconstructed images of the orthogonal projections for the PP-A sheet printed with the (1) aqueous and (2) solvent inks.

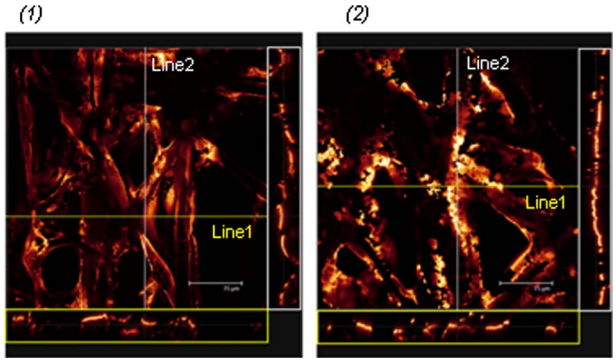

Figure 9. The reconstructed images of the orthogonal projections for the PP-AC sheet printed with the (1) aqueous and (2) solvent inks.

CONCLUSION

The absorption rates into three substrates for two different inks are predicted, within expected accuracy, by Darcy's Law combined with the Laplace equation. A range of contact angles, permeabilites, pore sizes, and void fractions is covered. The basic mechanism of capillary driven flow in porous media is confirmed. Pigments are captured in distinct layers for solvent inks. For aqueous inks, only the substrate coated with latex could capture pigments near the surface; this capture seems to be linked to the finer pore space generated by the latex.

REFERENCES

[1] F. A. L. Dullien, *Porous Media-Fluid Transport and Pore Structure*, 2nd ed. (Academic, New York, 1992).
[2] D. W. Bousfield, "Three dimensional modeling of short time fluid absorption in layered porous materials", *Fifth International Paper and Coating Chemistry Symposium* (Pulp and Paper Research Centre of Canada, Montreal, Canada, 2003) pp. 253–258.
[3] D. W. Bousfield and G. Karles, "Penetration into three-dimensional porous structures", J. Colloid Interface Sci. **270**, 396 (2004).
[4] M. C. Beland and P. J. Mangin, "Three-dimensional evaluation of paper surface using confocal microscopy", *Surface Analysis of Paper* (CRC Press, USA, 1995), pp. 1–40.
[5] M. C. Beland, S. Lindberg, and P. A. Johansson, "Optical measurement and perception of gloss quality of printed matte-coated paper", J. Pulp Pap. Sci. **26**, 120 (2000).
[6] Y. Ozaki, D. W. Bousfield, and S. M. Shaler, "Three-dimensional characterization of ink vehicle penetration by confocal scanning laser microscope", J. Pulp Pap. Sci. **31**, 48 (2004).
[7] Y. Ozaki, D. W. Bousfield, and S. M. Shaler, "Observation of the ink penetration in the coated paper by confocal scanning laser microscope", *TAGA Annual Conference Proceedings* (TAGA, Atlanta, GA, 2005) pp. 68 and 69.
[8] A. R. Dickson, "Quantitative assessment of ink pigment position within the surface of a newsprint sheet", Appita J. **58**, 272 (2005).
[9] T. Enomae, D. Ivutin, and A. Isogai, "Three-dimensional distribution of ink jet inks in paper acquired by confocal laser scanning microscope", *58th APPITA Annual Conference and Exhibition Proceedings*, (APPITA, Canberra, Australia, 2004), pp. 577–588.
[10] H. Hamada and Y. Ozaki, "Observation of the distribution of ink on non-cellulose fibers by confocal laser scanning microscope", Nord. Pulp Pap. Res. J. **21**, 558 (2006).
[11] H. Hamada, Y. Ozaki, and M. Naito, "Printability of ink jet printing on surface-treated nonwoven fabrics", *Proc. IS&T's NIP23* (IS&T, Springfield, VA, 2007) pp. 608–612.
[12] E. H. K. Sterlzer, "The intermediate optical system of laser scanning confocal microscopes," *Handbook of Biological Confocal Microscopy* (Plenum Press, New York, 1995) pp. 139–153.
[13] H. F. Jang, A. G. Robertson, and R. S. Seth, "Optical sectioning of pulp fibers using confocal scanning laser microscopy", Tappi J. **74**, 217 (1991).
[14] H. F. Jang, A. G. Robertson, and R. S. Seth, "Transverse dimensions of wood pulp fibers by confocal laser scanning microscopy and image analysis", J. Mater. Sci. **27**, 6391 (1992).